PHYSICAL REVIEW C VOLUME 8, NUMBER 3 SEPTEMBER 1973

Complete Hydrogen and Helium Particle Spectra from 30- to 60-MeV Proton Bombardment of Nuclei with $A = 12$ to 209 and Comparison with the Intranuclear Cascade Model*

F. E. Bertrand and R. W. Peelle
Oak Ridge National Laboratory, Oak Ridge, Tennessee 37830

(Received 30 March 1973)

Differential cross sections for the production of proton, deuteron, triton, helium-3, and α particles from as many as 10 targets ($A = 12$–209) were measured using 29-, 39-, and 62-MeV incident protons. The particles were detected, with ≈ 0.2-MeV [full width at half maximum (FWHM)] energy resolution for protons, over a secondary energy range of ≈ 2–6 to 62 MeV in a total absorption telescope composed of three solid-state detectors. Representative results are shown for cross sections differential in energy and angle, as well as for angle- and energy-integrated cross sections. For incident 60-MeV protons the integral magnitude of the nonevaporation charged-particle production is found to be $\sim 10^2 A^{1/3}$ mb. Fewer protons but more complex particles were measured for carbon and oxygen targets than expected from an $A^{1/3}$ dependence for either component alone. The continuum cross sections for $z = 1$ particles at a given angle (mb sr^{-1} MeV^{-1}) are nearly independent of incident energy when measured with incident protons in the 30- to 60-MeV energy range. Nonevaporation production of complex particles ($A \geq 2$) is 25-40% of that for protons. The proton spectra have been compared with predictions from the intranuclear cascade model. Differential spectral predictions compare well with the measured spectra for angles in the range ~25–60°, and relatively poor predictions for small and large angles are more favorable when reflection and refraction by the potential well are included. Evidence is given that predictions for backward angles are greatly improved by allowing proton scattering from nucleon pairs within the model nucleus, but the A-dependent underprediction at extreme forward angles is not understood at all. The calculated angle-integrated spectra reproduce the measured spectral shape but consistently predict $\approx 30\%$ too few nonevaporation protons for targets with $A \geq 27$.

NUCLEAR REACTIONS ^{12}C, ^{16}O, ^{27}Al, ^{54}Fe, ^{56}Fe, ^{60}Ni, ^{89}Y, ^{120}Sn, ^{197}Au, ^{209}Bi, $(p,p'X)$, (p,dX), (p,tX), $(p,{}^3\mathrm{He}X)$, $(p,\alpha X)$, $E = 62$, 39, 29 MeV; semi; measured $\sigma(E;\, E_{p'}, E_d, E_{^3\mathrm{He}}, E_\alpha, \theta)$; deduced $\sigma(E)$. $2 \lesssim E_{p'}, E_d, E_t, E_{^3\mathrm{He}}, E_\alpha \lesssim 70$ MeV. Comparisons with intranuclear cascade model.

I. INTRODUCTION

In this paper we present the results of an experiment designed to study the energy spectra of secondary proton, deuteron, triton, helium-3, and α particles produced by 62-, 39-, and 29-MeV proton bombardment of targets selected to cover a broad mass range. Spectra were obtained at many angles with narrow energy resolution over the secondary-particle energy range from ~2–62 MeV. The data provide differential cross sections, angle-integrated spectra, energy-integrated angular distributions, and integral particle production cross sections. Since most of the data were taken with 62-MeV incident protons, we emphasize the systematics of these results and use the data from lower incident proton energies mainly for comparative purposes. No spectroscopic results from these data are discussed here; however, some have previously been published.[1-3]

We use the notation $\sigma_{p,xd}(E', \theta)$, for example, to represent the doubly differential cross section for emission of a deuteron into the indicated energy and solid angle ranges, regardless of what other particles or photons may be emitted in the same reaction. Note that $\iint dE' d\Omega \sigma(E',\theta) \equiv Y_d \sigma_R$, where σ_R is the reaction cross section for the incident protons and Y_d is the mean yield or multiplicity of deuterons. We use the term continuum to describe the region of the secondary-particle spectra which lies between the peaks from excitation of low-lying residual nucleus levels and the low-energy "evaporation" peak or the Coulomb cutoff.

A. Earlier Measurements

Over the past several years many papers have described inelastic scattering and pickup reactions of medium-energy incident protons leading to bound states of residual nuclei. For incident protons with $E \gtrsim 50$ MeV, the bound-state region of the secondary charged-particle spectra includes only a small part of the total charged-particle emission cross section; yet few experiments have been performed to study the high-excitation regions. The few earlier continuum measurements have generally concentrated on the outgoing proton spectrum and have nearly always omitted important parts of the energy range of the emitted particles.

Studies of the proton spectra resulting from 200- to 1000-MeV proton bombardment[4-7] have generally shown the presence of a broad peak from quasifree proton-nucleon scattering. These spectra have been rather well described by calculations.[8,9] Experiments have also been performed to study the deuteron continuum from 340-MeV[10] and ≈1-BeV[11,12] proton bombardment.

Experimental studies of the inelastic[13-23] and complex-particle[14,24-27] ($d, t, \ldots$, etc.) continuum spectra have been more numerous using 30- to 200-MeV protons. These experiments have generally covered only a small part of the range of secondary energy, solid angle, or target mass. The results from the earlier experiments have led to proposed reaction mechanisms which are incorporated into widely used reaction models and calculational methods.[8,9,28-30] Our detailed results support most of the earlier observations, although we find some differences which have come about mainly by the lack of complete studies.

B. Models

Proton Inelastic Continuum

A few calculational models have been proposed which attempt to represent parts or the whole of the inelastic continuum. Two models are at present extensively used to calculate the entire secondary inelastic spectra: the preequilibrium statistical model initially proposed by Griffin[28] and the intranuclear cascade (INC) model first proposed by Goldberger[31] and computerized by Metropolis *et al.*[32]

Recently some comparisons[33-35] have been made to our experimental results using the preequilibrium statistical model. The present preequilibrium models are confined to angle-integrated spectra and only the "hybrid"[33,34] versions provide absolute cross sections. One version of the model includes an extension to account for complex-particle emission.[35]

Kroll and Wall[9] have attempted to describe the quasifree scattering processes in significant detail using a distorted-wave Born-approximation (DWBA) formalism. While their results give encouraging agreement with the data of Wall and Roos[18] at 160 MeV and of Corley *et al.*[4] at ≈1 BeV, their calculation deals only with single interactions within the nucleus.

In this paper we present comparisons of our proton continuum measurements with the intranuclear cascade (INC) model. While there are presently three widely used versions of the model, due to Bertini,[36] Barashenkov, Gudima, and Toneev,[37] and Chen *et al.*,[38] we generally present results from the calculations of Bertini but briefly discuss some comparisons with the model of Chen. A comparison of the results from these three models has recently been published.[39] We discuss below some of the basic tenets of the model.

The cascade model, below the meson-production threshold energy, assumes that the interaction with a real nucleus can be replaced by a sequence of nucleon-nucleon interactions within a model nucleus. The collisions between the nucleons are treated as free-particle collisions except for an approximate exclusion principle, and the scattering kinematics are selected by Monte-Carlo sampling. The nucleon products from each initial INC collision are followed in the nucleus and one or both of the products are allowed to escape directly [e.g., (p, p'), $(p, 2p)$] or collide again. (The term "quasifree", sometimes "quasielastic", is used to describe the scattering process in which a nucleon escapes after one intranuclear collision.) If one of the initial products is not emitted, a second collision may occur and the continuation of this process can result in a "cascade" of nucleons moving through the nucleus. The importance of particle emission following secondary INC collisions is demonstrated by the Bertini model prediction that for 62-MeV incident protons only ~60% of the integral proton cascade yield comes from protons emitted from the initial collision. For 39-MeV protons initial collision emission accounts for ~65% of the integrated proton yield. The cascade terminates when no more cascade nucleons have energy above a predetermined cutoff energy since the cascade process does not allow the excitation energy of a hole or of two particles to be reshared to give one outgoing particle. The remaining excitation energy of the nucleus is then assumed to be widely distributed, and the excitation energy is released through an "evaporation" process.

These cascade models approximate the nucleon density distribution by a series of annular spherical regions, with the well depth in each region chosen so that degenerate neutron and proton Fermi gases have the proper densities in each region if the minimum separation energy is taken for instance as 7 MeV. In the case of the Bertini calculation, three spherical regions are used, while the version by Chen uses eight regions. Earlier cascade models employed uniform density distributions (square potential wells) and yielded markedly inferior results.[36] Table I lists the well depths and radii used in the calculations for 62-MeV protons on ^{12}C, ^{54}Fe, and ^{209}Bi using the MECC3 code of Bertini.

TABLE I. Nuclear model parameters for intranuclear cascade calculations with the Bertini model for three of the target nuclei in this study. The concentric boundaries between the regions of constant density are taken to be the same for neutrons and protons. The potentials and Fermi-gas densities given correspond to a 7-MeV separation energy for the least bound nucleons.

Nucleus	Outer radius of region (fm)	Proton [a] Density (10^{36} cm^{-3})	Proton [a] Potential (MeV)	Neutron [a] Density (10^{36} cm^{-3})	Neutron [a] Potential (MeV)
^{12}C	1.31	62.4	−38	62.4	−38
	3.22	31.3	−27	31.3	−27
	4.96	3.60	−12	3.60	−12
^{54}Fe	2.85	76.0	−43	82.9	−45
	4.80	41.3	−31	44.5	−32
	6.55	4.63	−13	4.98	−13
^{209}Bi	5.16	70.4	−41	106.8	−52
	7.11	39.1	−30	59.3	−37
	8.86	4.36	−12	6.62	−14

[a] Potential and density in region between radius edges (e.g., for ^{12}C in the region bounded by 0–1.31 fm, the proton potential is −38 MeV).

While the incident or exit nucleon gains or loses kinetic energy in crossing each potential boundary within the model, the Bertini version of the INC provides no change in the particle's direction by refraction or reflection. In the Chen version (VPOT = 0.5), these deflections are allowed as computed on a classical basis. Comparisons to spectra from ~50-MeV incident nucleons, such as that presented here, might be expected to indicate the importance of refraction and reflection in the model.

Since the energy resolution in this experiment was rather narrow, strong peaks induced by inelastic scattering to discrete levels dominate the highest energy portion of the observed spectra at angles less than ~60°. These strongly excited levels are normally described as collective excitations ("vibrations"), but the INC model cannot explicitly describe such excitations. The excitations in the INC model are single-particle excitations although the use of a model based on a Fermi gas prevents reproduction of any level structure. However, in an average way in which collective levels are imagined to be decomposed into a continuum of single-particle excitations, the cascade model cross section can be thought to represent the cross section averaged over energy regions broad compared to the level spacing of the important collective excitations. In any case the total collective strength localized in the bound-state region of the inelastic spectra is only a few percent of the total cross section for proton emission for the incident energies studied in this work.

The evaporation calculation used by Bertini to allow deexcitation of the post-cascade nucleus is based on a Monte-Carlo computer program by Dresner[40] to evaluate the Weisskopf nuclear evaporation process[41] following the techniques of Dostrovsky, Frankel, and Friedlander.[42] This calculation uses inverse cross sections from the Dostrovsky prescription, rather than those from the optical model, and does not recognize or conserve angular momentum. The excitation energy used in the evaporation calculation is that remaining after the completion of the cascade process. Thus, if an incorrect amount of energy emission is predicted for the cascade products (the general case at 60 MeV), the evaporation program will predict the wrong low-energy cross section.

Since it has long been proposed that the INC model is primarily applicable for incident nucleon energies above ≈150 MeV,[36] it seemed of interest to test the model at energies well below its nominal range. Such a test may be particularly timely in that the cascade model is now being used to calculate the charged-particle and neutron spectra from pion capture in complex nuclei, and these calculations directly involve the use of the cascade model for effective incident nucleon energies ≲ 70 MeV.[43]

Complex-Particle Continuum

While the INC model predicts a wide variety of quantities for incident and exit nucleons and mesons, the model at present cannot account for incident or exit complex particles. (Complex particles are produced in the evaporation portion of the combined model). It will be shown that even at 60 MeV, nonevaporation complex-particle production is a significant fraction of the proton production. In a recent publication by Kalbach-Cline,[35] the preequilibrium statistical model has been applied to our measured, angle-integrated complex-particle spectra with encouraging results, but very little theoretical effort has been expended toward any microscopic description of the complex-particle continuum.

The bound states excited in few nucleon pickup or stripping reactions have been well explained for some time by the direct pickup reaction calculated by the DWBA method. In a forthcoming paper[44] it will be shown that the direct pickup mechanism accounts for only a small fraction of the total deuteron spectrum produced by 60-MeV protons. At energies above ~300 MeV, a few attempts have been made to explain deuteron continuum spectra. The most often used model involves indirect pickup,[10,11,45,46] a higher-order process in which, for example, an incident proton scatters as in the INC model and then picks up a neutron.

II. EXPERIMENT

The entire data acquisition and analysis system has been described in detail.[47-49] Protons were accelerated by the Oak Ridge isochronous cyclotron, momentum analyzed to ≈0.1% in momentum, and focused on the targets (thickness 1–10 mg/cm^2) in a spot ≈8 mm in diameter. Data were taken using 62-, 39-, and 29-MeV incident protons. Proton, deuteron, triton, helium-3, and α particles emitted from the target were detected in a three-counter telescope composed of two silicon surface-barrier detectors (≈100μm, ≈500μm) and a lithium-drifted germanium stopping detector.[50] The secondary charged particles were unambiguously identified by $\Delta E \times E$ and flight time vs E methods over an energy range from a few[51] MeV to 62 MeV (see Ref. 47). The detector system contributed an energy resolution of ≈0.2 MeV (FWHM) for 62-MeV protons; however, a resolution of ≈55 keV was obtained with the Ge(Li) detector used alone. Data were obtained from four analog-to-

TABLE II. Targets, projectile energies, numbers of angles of observation, and report numbers for tabulated data and detailed experimental discussion.

Target	E(proton) (MeV)	Number of angles	ORNL Report No.
^{209}Bi	62, 39	18, 4	4638 (1971)
^{197}Au	62, 29	6, 4	4460 (1969)
^{120}Sn	62, 39	20, 5	4471 (1970)
^{89}Y	62	5	4450 (1969)
^{60}Ni	62	4	4698 (1971)
^{56}Fe	62	13	4456 (1969)
^{54}Fe	62, 39, 29	24, 7, 7	4469 (1970)
^{27}Al	62, 29	18, 3	4455 (1970)
^{16}O	62, 39, 29	18, 4, 1	4799 (1973)
^{12}C	62, 39, 29	19, 5, 2	

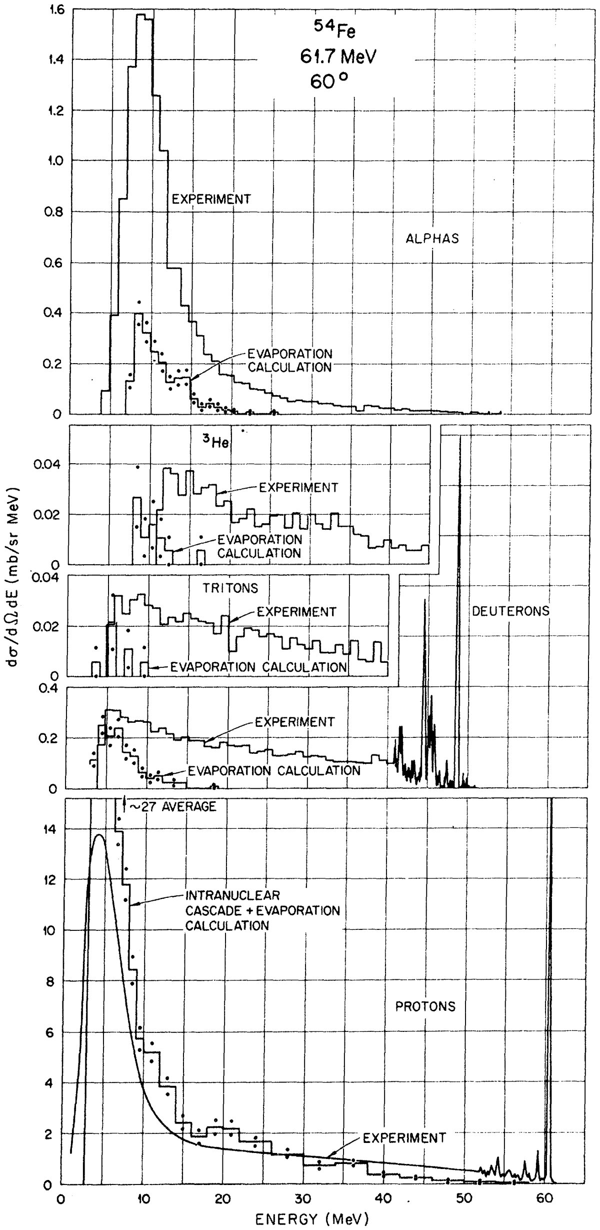

FIG. 1. Charged-particle spectra from ^{54}Fe at 60° compared with the intranuclear cascade plus evaporation calculation. The measured proton spectrum is shown as a smooth curve for energies below the peaks from inelastic scattering to discrete states, while the other measured particle spectra are shown binned in 1-MeV bins for energies below the discrete peaks. The calculated spectra from the Bertini model are shown as a histogram with "dots" indicating Monte-Carlo statistical uncertainties.

digital converters for each event, processed and written onto magnetic tape by an on-line PDP-8 computer, and later analyzed on the laboratory's IBM-360 computer and on the PDP-8.

We have published a series of Oak Ridge National Laboratory reports[49,52] which give the (binned) experimental data and uncertainties in tabulated form and describe any special corrections required for data from each of the ten targets. The systematic uncertainty on the results ranges from 5–10%; this uncertainty should be combined with the statistical uncertainties shown in most of the plots. Table II lists the targets studied, the incident proton energies, the number of angles of observation, and the report number in which the tabulated data are available.

The data have been corrected to remove in first order the effects of energy loss of scattered particles in the target and in the nickel window "dead" layer covering the germanium detector, penetration of the edges of the detector collimator, multiple scattering of secondary protons by the ΔE detectors, and nuclear reactions of hydrogen particles in the germanium detector. The correction techniques are described in detail in Refs. 47 and 49.

III. RESULTS AND COMPARISONS WITH THE INC MODEL

Figure 1 shows the ^{1}H, ^{2}H, ^{3}H, ^{3}He, and ^{4}He spectra from ^{54}Fe at 60° for 62-MeV incident protons. These results are examples of the types of data obtained for each target at each angle of observation. Due to the small cross sections and limited data collection time, ^{3}H, ^{3}He, and ^{4}He spectra generally showed little high-energy structure.

At energies below the marked high-energy peaks the spectra become rather smooth and structureless except for angles smaller than $\approx 35°$, and merge for the case of protons and α particles into a low-energy peak. The d, t, and ^{3}He spectra show relatively much less low-energy cross section than the proton and α-particle spectra show.

The calculated proton spectrum in Fig. 1 reproduces the measured spectral shape and magnitude quite well in the continuum region except that the predicted evaporation cross section is much too large. The INC model cannot at present provide complex cascade particles and the predicted complex-particle evaporation spectra fail to match the observed spectral shape for deuterons, tritons, and helium-3's. The comparisons shown in Fig. 1 indicate that nuclear evaporation is not the predominate mechanism in the production of these complex particles by 60-MeV incident protons. The predicted low evaporation magnitude for the α particles is found to be systematic in the calculation used. Since we wish to discuss mainly the high-energy spectra, these low-energy discrepancies will not be much discussed in this paper.

A. Secondary Protons

Differential Spectra

Figures 2–6 show the measured and calculated (p, xp) spectra at several angles from 62-MeV bombardment of ^{12}C, ^{27}Al, ^{54}Fe, ^{120}Sn, and ^{209}Bi.

The low-energy region of the spectra from ^{12}C, ^{27}Al, and ^{54}Fe is dominated by the apparent evaporation peak which is observed to have a nearly isotropic intensity. Earlier papers[16,17] reported that the evaporation contribution to the proton total inelastic cross section would be small; however, while this prediction is correct for heavy targets, Figs. 2–4 demonstrate the importance of evaporation for medium and light targets. For all the nuclides studied, the high-energy continuum decreases rapidly in magnitude with increasing angle; however, even at the largest angles there is a

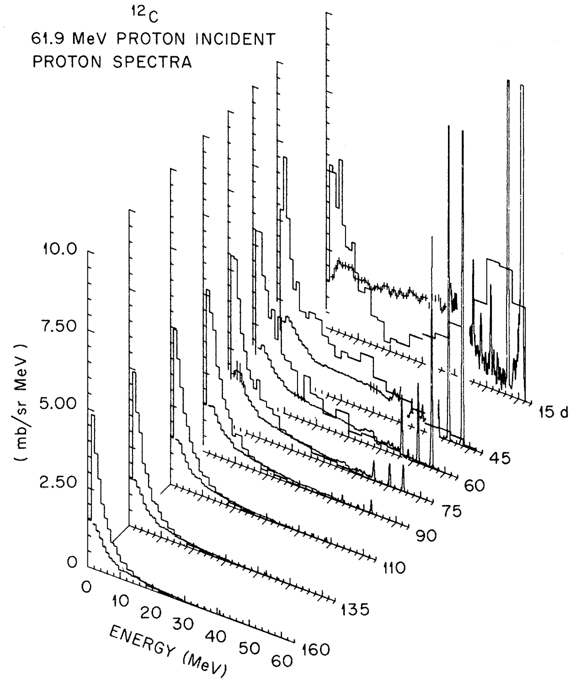

FIG. 2. ^{12}C(p,xp) spectra for incident protons of 61.9 MeV. The measured spectra are shown in bins for energies below the obvious discrete peaks. The Bertini intranuclear cascade plus evaporation model calculation is shown as a histogram with steps broader than those used for the data. Note that the high-energy peaks at small angles are often off scale. The uncertainties shown on the experimental data represent mainly statistical uncertainties and exclude 5–10% systematic uncertainties.

measurable cross section extending to the maximum kinematically allowed energy.

At angles less than ≈35°, a broad peak is consistently observed in the continuum with an excitation energy between 19 and 12 MeV for $A = 27-209$. Although such a peak is reminiscent of the quasifree peak well established for incident energies above 300 MeV, its excitation energy behavior rules out such a description. The peak, also observed with 185-MeV protons[21] and in recent (e, e') experiments,[53] has been interpreted as collective excitation of a giant quadrupole[3, 54] or possibly monopole[55] resonance. The absence of a quasifree peak in our data is in agreement with other measurements with incident protons of less than 100 MeV.[15, 16] There is conflicting experimental evidence for quasifree peak observation in the 160-MeV[17–20] region. χ^2 tests show that within the available statistical accuracy and resolution, no fine structure is observed in our continuum data except for the (p, np) peak in the 40-MeV ^{209}Bi data. (See ^{209}Bi report of Ref. 52.)

The accuracy of the INC model in representing experimental results is found to be strongly dependent on the angle of observation. Comparison of the calculation to observed differential spectra

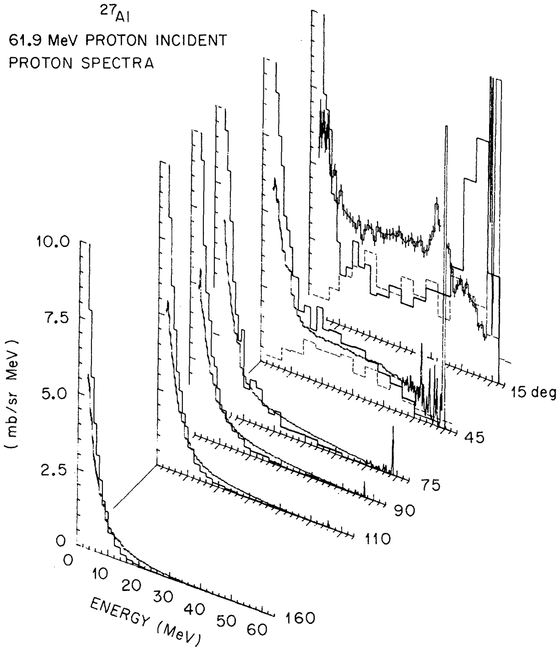

FIG. 3. ^{27}Al(p,xp) spectra. See Fig. 2 caption. The calculated evaporation cross section is off scale with maximum value ≈11. For the 15 and 45° spectra the solid broad-stepped histogram is the cascade calculation of Bertini and the dashed histogram is the cascade calculation of Chen *et al.* Note that the Chen calculation (using VPOT = 0.5) does not predict the strong quasifree peak predicted by Bertini but unobserved in the measurement. The calculated results of Chen *et al.* do not include any contribution from evaporation; thus comparisons with the data should be made only above ≈15 MeV. The broad peak in the data at ≈40 MeV is produced by collective excitation of the giant quadrupole resonance (see Refs. 3, 53, and 54).

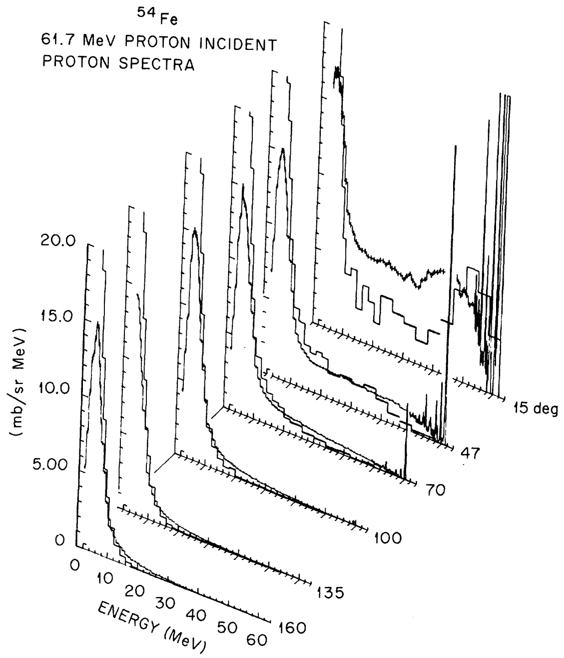

FIG. 4. ^{54}Fe(p,xp) spectra. See Fig. 2 caption. The calculated low-energy cross section is off scale with maximum value ≈29.

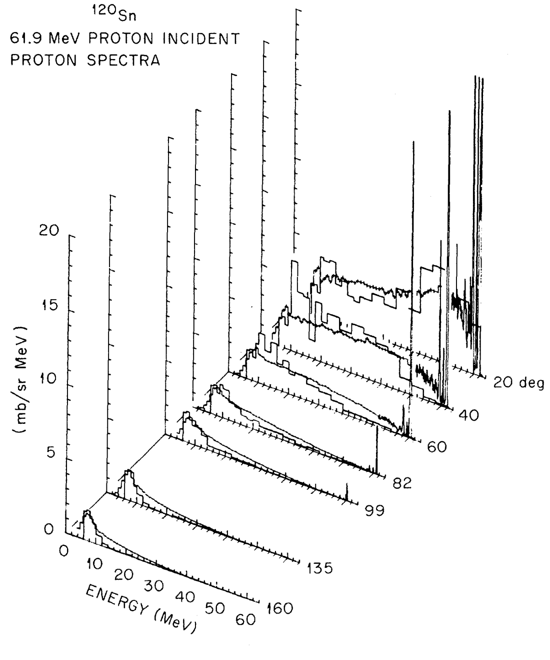

FIG. 5. ^{120}Sn(p,xp) spectra. See Fig. 2 caption.

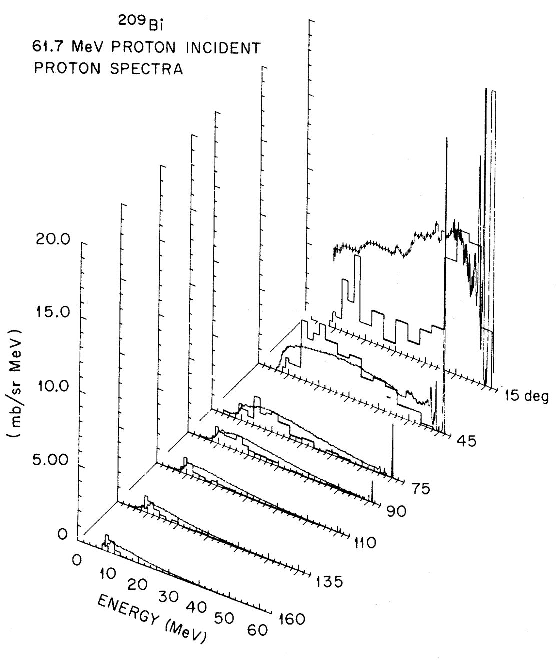

FIG. 6. ^{209}Bi(p,xp) spectra. See Fig. 2 caption.

represents a stringent test of the model in that the calculation must properly account for reaction mechanisms which have strongly different angular distributions. Model deficiencies often go undetected by use of only integral comparisons. In the angular range from ~20–60°, in which ~75% of the calculated integral cross section is located, relatively good agreement between the measurement and calculation is obtained. However, the agreement is poor at larger and smaller angles.

For each target the calculated 15° spectrum is dominated by a strong quasifree peak which is not observed in the data. As discussed in Sec. I, the INC model of Bertini does not consider deflection of the incident or exit particle trajectory, even though it has been well established that distortion effects are important in nuclear reactions below 150 MeV. We have tested the importance of this effect in the INC model by comparing[56] our data with the calculations of Chen *et al.*[38] The 15° data from 62-MeV protons on ^{27}Al are compared to the Bertini INC and the Chen INC calculations on Fig. 3. The importance of reflection and/or refraction in the INC model is demonstrated by the observa-

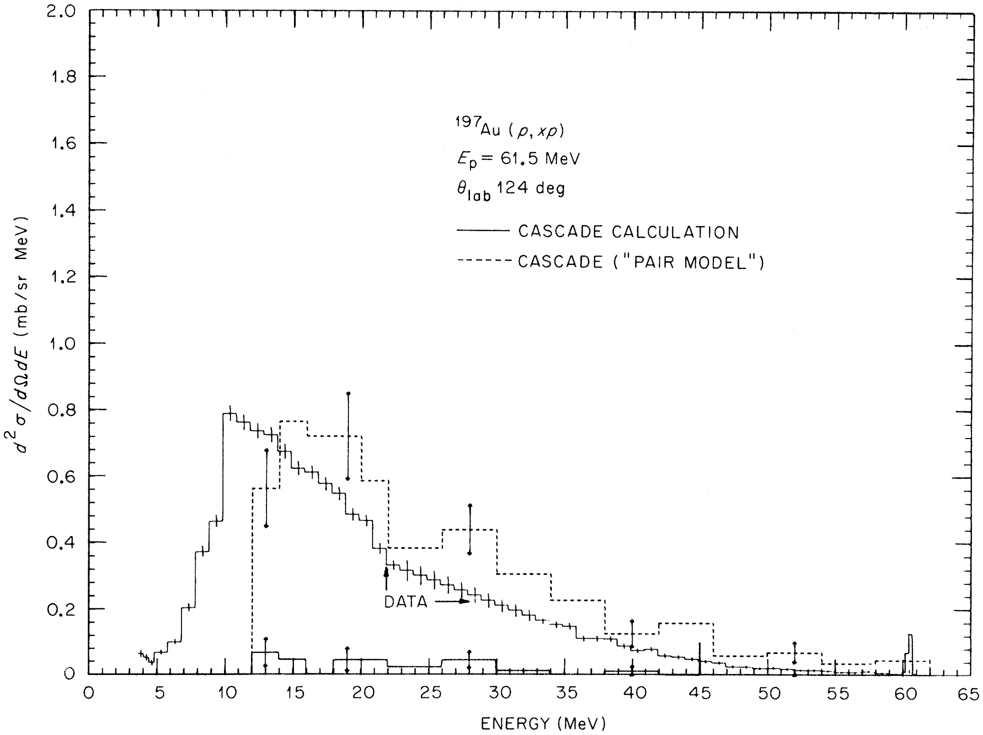

FIG. 7. ^{197}Au(p,xp) spectrum at 124° for E_p = 61.5 MeV. The experimental data are shown as a histogram with 1-MeV-wide bins, the standard Bertini INC calculations as a wider solid histogram, and the modified nucleon "pair model" as a dashed histrogram. The calculations did not include evaporation. The calculations did not include transport, "decay," or escape of the struck nucleon pair.

tion that the Chen calculation does not predict a quasifree peak when reflection and refraction are included, presumably because of the angle mixing. A similar comparison is shown for 45° and in this case the two calculations agree well. For targets heavier than Al, the Chen calculation with reflection and refraction badly underestimates the measured over-all spectral intensity.

Brun *et al.*[17] using 96- and 156-MeV protons on heavy targets found poor agreement with their data using reflection and refraction in the Chen (STEP) calculation. This observation was based only on magnitude comparisons since the poor energy resolution of their measurements prevented detailed high-energy spectral shape comparisons. While we too find poor agreement in magnitude for heavy targets, the small-angle spectral shape is consistently more reliably reproduced using reflection and refraction. However, both calculations badly underestimate the small-angle cross sections in the 15–40-MeV region of secondary energy.

For the largest angles of observation the Bertini calculation predicts that no cascade events occur ($\sim 10^{-4}$ of reactions for $\theta \gtrsim 125$; see Fig. 12), and the calculated results are entirely from the evaporation part of the calculation. The Chen version with reflection and refraction provides more backward-angle cross section, although still an order of magnitude too little. This backward-angle prediction is increasingly inconsistent with the measured spectra for heavier targets. Brun *et al.*,[17] Dubost *et al.*,[24] and Peelle *et al.*[19] observed similar high-energy "tails" at backward angles using ~156-MeV protons. Recent (p, xn) data[57] at ~65 MeV show measurable high-energy neutron cross section at backward angles, again inconsistent with the INC prediction.

The INC model assumes that all interactions take place between "free" nucleons. Since the existence of strongly correlated pairs of nucleons within the nucleus has been inferred experimentally[12] by the observation of knockout of quasifree deuterons from complex nuclei, the use of different scattering kinematics within the INC model could represent scattering of nucleons by nucleon pairs. With Bertini,[58] we have compared in Fig. 7 a preliminary nucleon-pair calculation with our results for ^{197}Au(p, xp) at 62 MeV for 124°. The good agreement shown is fortuitous since the assumption that all collisions occur with nucleon pairs is unrealistic. Further, the same calculation does not give as good agreement at smaller angles as does the standard version. In order to account for the backward neutrons by collisions with nucleon pairs, it would be necessary to appeal to charge-exchange interactions.

Figures 8 and 9 show the differential spectra at

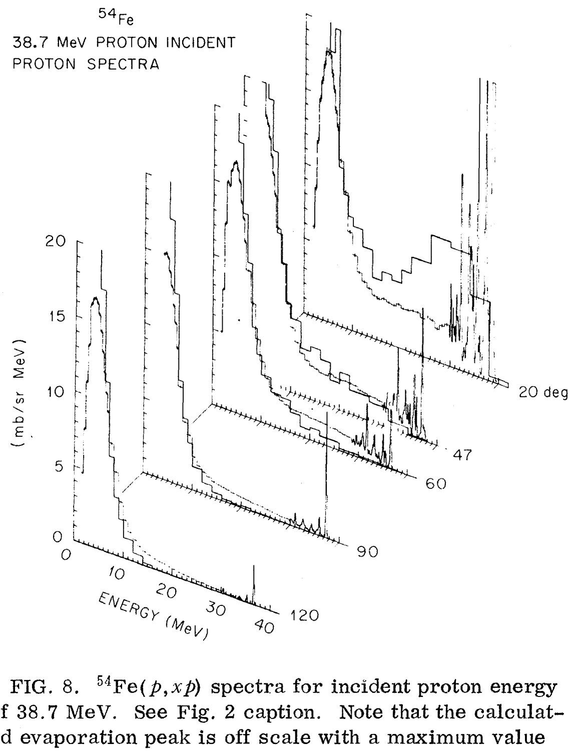

FIG. 8. ^{54}Fe(p,xp) spectra for incident proton energy of 38.7 MeV. See Fig. 2 caption. Note that the calculated evaporation peak is off scale with a maximum value of ≈30.

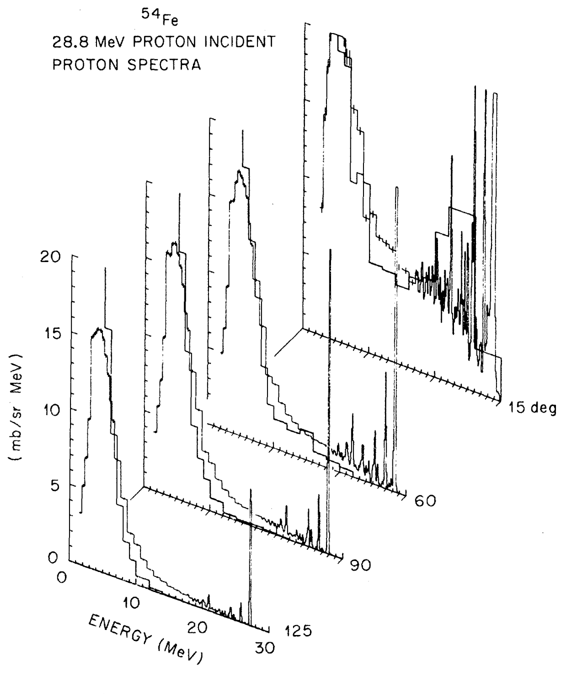

FIG. 9. ^{54}Fe(p,xp) spectra for $E_p = 28.8$ MeV. See Fig. 2 caption. Note that the calculated evaporation peak is off scale with a maximum value of ≈30.

several angles for secondary protons from ^{54}Fe bombarded by 38.7- and 28.8-MeV protons, respectively. The trends of the data at lower bombarding energies are found to be similar to those at 62 MeV. The cross section in the continuum for ^{54}Fe at a given angle for the three incident energies remains approximately constant over this energy range. The same is true for comparisons for other targets and secondary particles. The conclusion that the inelastic continuum cross section is a very slowly varying function of projectile energy is supported by the observation that for 160-MeV incident protons,[18,19] the average continuum cross section per MeV in the 20–40° angle range decreases only 20–30% from our 60-MeV cross sections. Since the reaction cross section does not change greatly between 60 and 160 MeV, the yield of cascade protons must increase for higher energies to account for the larger integral proton cross section.

The angular behavior and quality of comparisons with the calculated cascade spectra for the lower incident energies is found to be similar to that noted at 62 MeV, except that the predicted cross section at small angles is now almost completely dominated by the quasifree peak.

Figures 10 and 11 show the experimental angle-integrated spectra compared with the intranuclear cascade plus evaporation model for 62- and 39-MeV incident protons, respectively. Our comments refer to that part of the spectra above 20 MeV. The calculation in all cases reproduces the measured integral spectra reasonably well with the largest disagreement for Sn and Bi. There is at most 1–2 MeV difference between measured and calculated average spectral energies. The calculated intensity is low for heavy and medium mass targets while in good agreement with the results for light targets.

Angular Distribution

The $E > 20$-MeV proton angular distributions from five targets are compared with the prediction of the Bertini INC model on Fig. 12. We assume

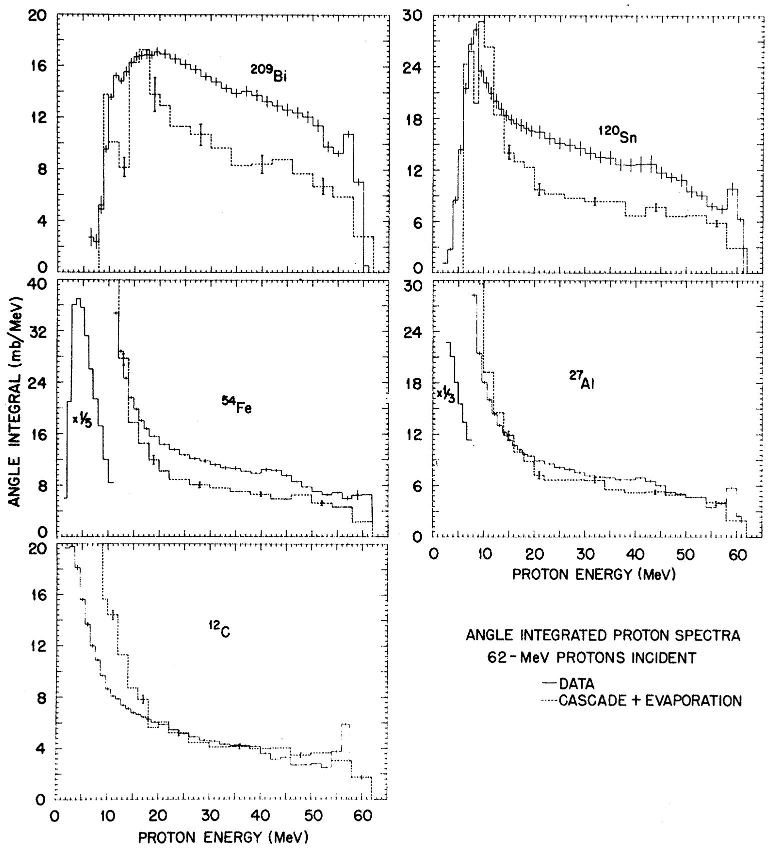

FIG. 10. Measured and calculated (Bertini INC model) angle-integrated laboratory proton spectra from 62-MeV protons on ^{12}C, ^{27}Al, ^{54}Fe, ^{120}Sn, and ^{209}Bi. The spectra exclude elastic scattering. Note that the calculated low-energy spectra for ^{54}Fe, ^{27}Al, and ^{12}C are off scale with maximums at ≈365, ≈138, and ≈65, respectively. The measured low-energy spectra for ^{54}Fe and ^{27}Al have been plotted on reduced scale as shown. The calculations for Bi and Sn reflect the choice of Coulomb thresholds applied in the cascade calculation.

that the Dostrovsky evaporation theory describes the shape of the low-energy spectrum; therefore, the 20-MeV cutoff ensures that no evaporation contribution to the data or calculation is included. The angular distributions follow the trends observed in the differential spectra, showing strong forward peaking with a more constant cross section at backward angles. Note that the measured small-angle increase in cross section becomes greater as the target mass increases, a trend not followed by the INC calculation. Similarly shaped angular distributions have been obtained at other incident energies[16,17,24] utilizing more limited ranges of secondary energy and angle of observation.

These results show that a "smearing out" of the predicted quasifree peak would not provide enough cross section at small angles to agree with experiment. The rapid rise in the measured small-angle continuum cross section, which is increasingly important for large A, is a primary qualitative result which begs theoretical description. Very considerable experimental efforts were expended to assure that the small-angle spectra are not compromised by spurious events. This behavior has proved quite important in the correction of experimental reaction cross-section data.[59]

B. Production of Complex Secondary Particles

Figures 13–17 show several examples of the complex-particle differential spectra. For each particle type the cross sections exhibit a strongly forward-peaked high-energy continuum region. The spectra in the case of the ^{54}Fe$(p, x\alpha)$ results, while showing a distinct high-energy cross section, are dominated by a nearly isotropic low-energy peak from evaporation and/or higher-order preequilibrium emission (see Ref. 35). Except possibly for the $(p, x\alpha)$ spectra from light and medium mass targets, the whole of our data for production of d, t, ^{3}He, and ^{4}He shows that the evaporation mechanism is unimportant at this incident energy. Gadioli *et al.*[60] in a recent analysis of the ^{209}Bi(p, α) reaction at 30, 35, 40,

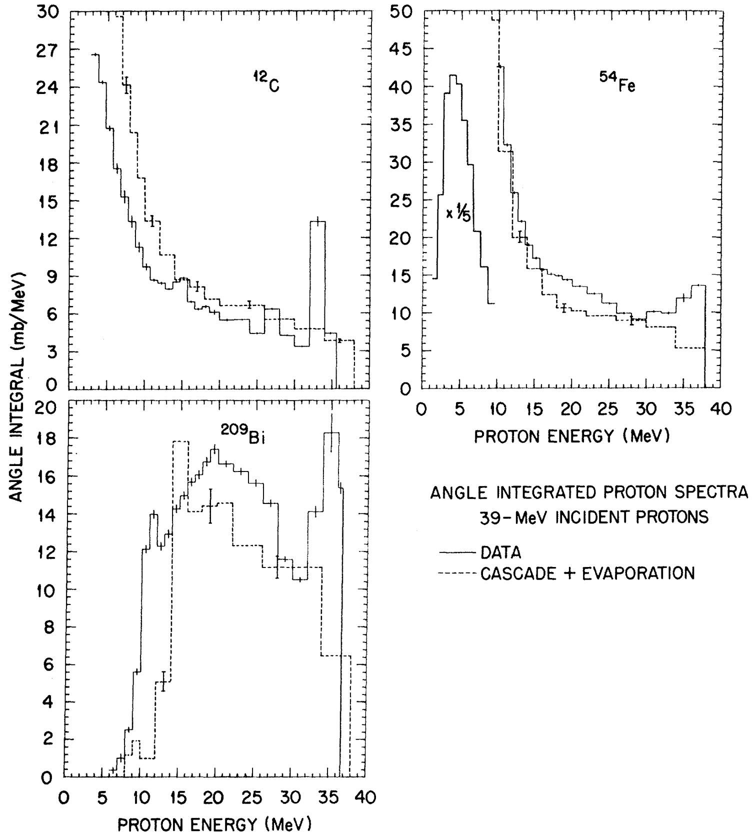

FIG. 11. Measured and calculated (Bertini INC model) angle-integrated laboratory proton spectra from 39-MeV protons on ^{12}C, ^{54}Fe, and ^{209}Bi. The spectra exclude elastic scattering. The calculated low-energy spectra for ^{12}C and ^{54}Fe are off scale with maximum at 94 and 380, respectively. The measured ^{54}Fe low-energy spectrum has been plotted on a reduced scale as shown. The prominence of the high-energy peak structure is caused to some extent by the availability of data from only 5–6 angles to estimate the angle-integrated spectra.

and 44.5 MeV also find that only ≈10% of the integrated α-particle cross section is accounted for by "statistical" processes. On the other hand, the major cascade models presently in use allow emission of complex particles only through the evaporation process which yields spectral shapes, angular distributions, and integral cross sections completely inconsistent with our measured results. Thus, in this energy region the cascade plus evaporation model does not at all represent the spectral shape or magnitude of the observed emission of complex particles.

The ^{209}Bi(p, xd) spectra presented on Fig. 13 show the presence of a broad peak at ~50 MeV, ~6 MeV of excitation. The peak is observed for angles smaller than ~35° and increases in magnitude with decreasing angle of observation more rapidly than the continuum at higher excitation energy. The excitation energy and width of the peak, the peak cross section, and the gap in cross section between the strong multiplet peaks from valence shell neutron pickup suggest that the ob-

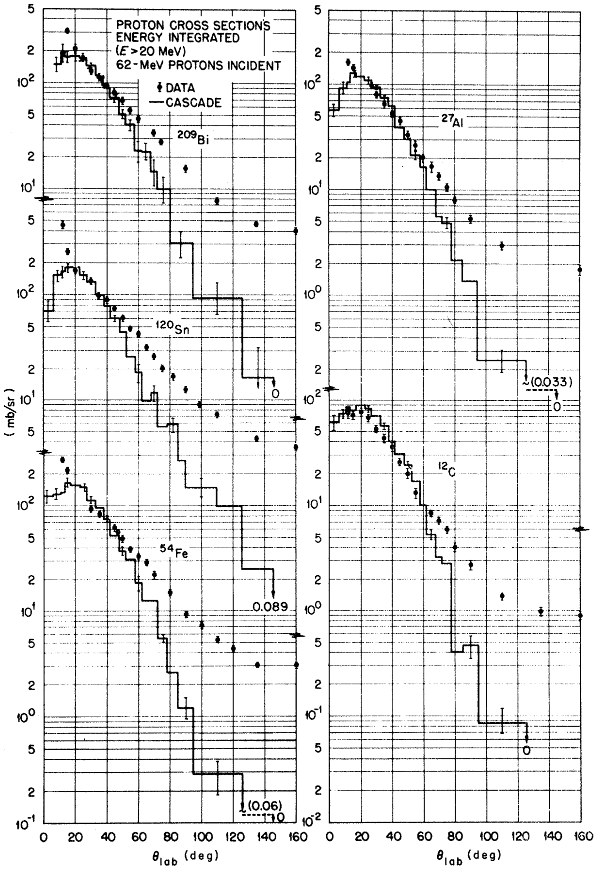

FIG. 12. Angular distributions for protons with $E \gtrsim 20$ MeV from 62-MeV proton bombardment of ^{12}C, ^{27}Al, ^{54}Fe, ^{120}Sn, and ^{209}Bi. The 20-MeV low-energy cutoff ensures that no evaporation contribution is made to the data or calculation. Elastic scattering is not included in the data. The histogram corresponds to the Bertini INC model.

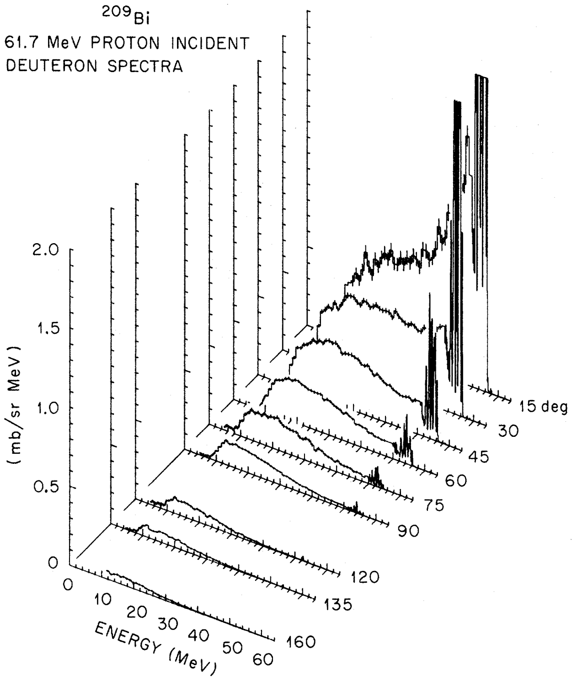

FIG. 13. Measured ^{209}Bi(p,xd) spectra for $E_p = 61.9$ MeV. The high-energy peaks are off scale at the small angles.

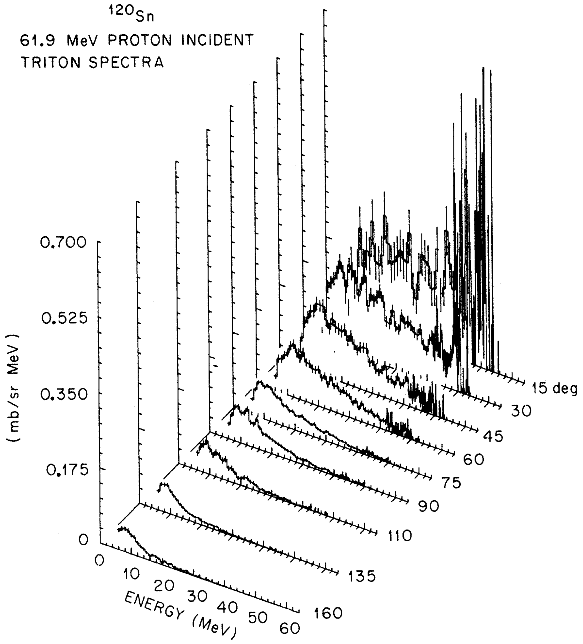

FIG. 14. Measured ^{120}Sn(p,xt) spectra for $E_p = 61.7$ MeV.

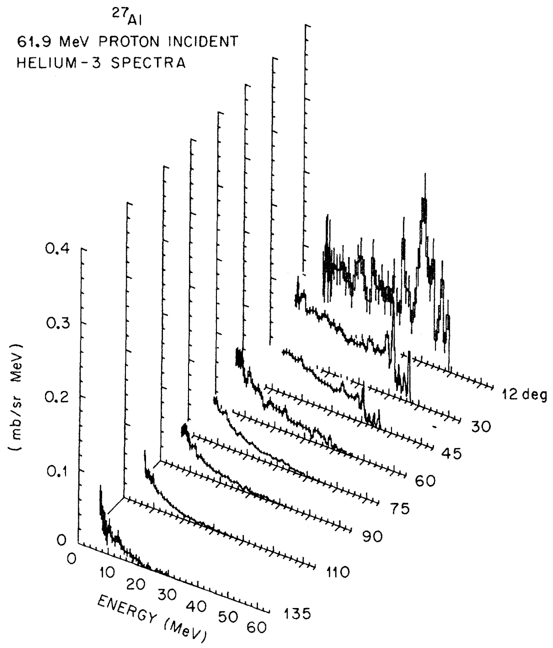

FIG. 15. Measured ^{27}Al(p,x^3He) spectra for E_p =61.7 MeV.

served enhancement is provided by inner shell (50-82 shell) neutron pickup. We observed similar structure in the ^{120}Sn(p, xd) spectra. Detailed analysis of these (p, xd) results will be presented elsewhere.[44]

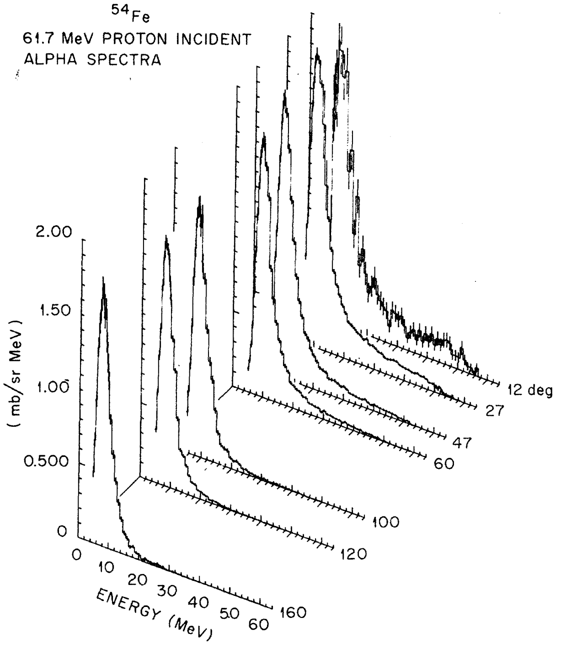

FIG. 16. Measured ^{54}Fe(p,$x\alpha$) spectra for E_p =61.7 MeV.

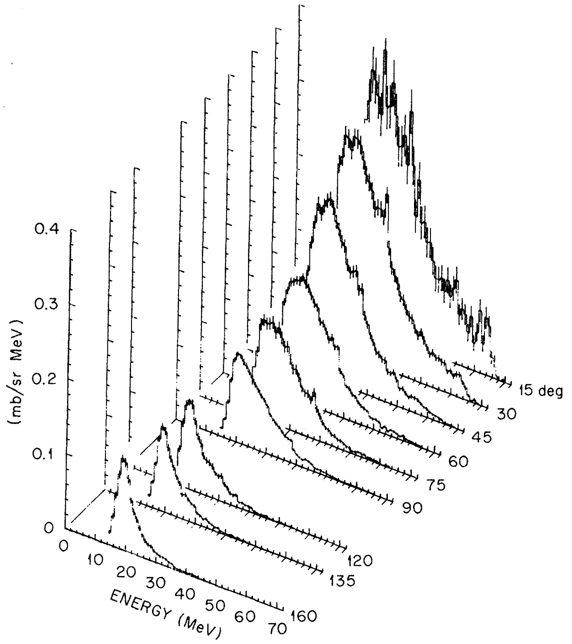

FIG. 17. Measured ^{209}Bi(p,$x\alpha$) spectra for E_p=61.7 MeV. The apparent structure near 37 MeV is introduced by imperfections in the correction of the data for the 3-mg/cm^2 nickel window which covers the Ge detector.

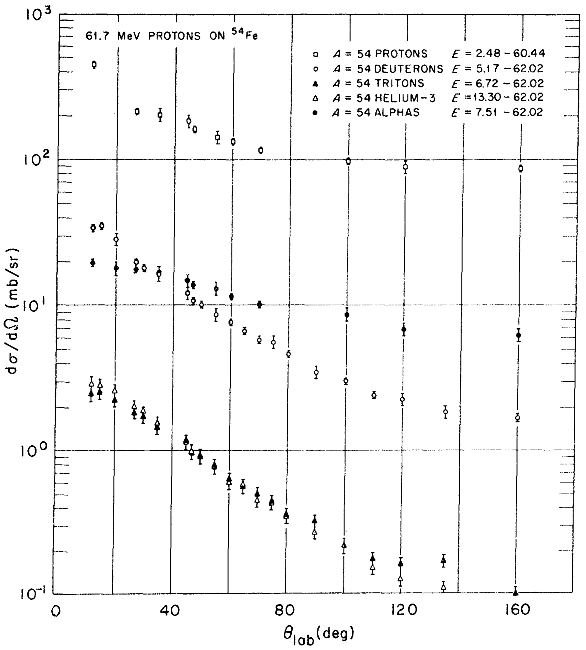

FIG. 18. Angular distributions of charged particles emitted by ^{54}Fe bombarded by 61.7-MeV protons. The cross sections at each angle are from the sum of the spectral intensity over the energy range shown for each particle type. The proton results exclude elastic scattering, while the complex-particle results are summed over the entire measured spectrum.

The Ag(p, xt) reaction by Dubost *et al.*[25] at higher incident energies showed a low-energy peak characterized by a double maximum. Such a distribution was not observed in any of our triton data which is typified by the ^{120}Sn(p, xt) spectra in Fig. 14.

Figure 18 shows the energy-integrated angular distributions of p, d, t, ^{3}He, and α particles from ^{54}Fe at 62 MeV. The energy cutoffs (shown on the figure) include nearly all nonelastic particle emission except for ^{3}He. These results are typical of those from all targets except that the evaporation contribution to the cross section for heavy targets is small. The figure illustrates the smooth behavior of the cross section with angle and the general similarity between the angular distribution shapes for the various particle types. At angles less than ~90° the angular distributions for all particle types are similar with strong forward peaking. When the evaporation process is observed to provide an obvious contribution to the spectra (e.g., secondary proton spectra from ^{54}Fe), the process is reflected in the nearly isotropic character of the angular distributions for angles greater than ~90°.

The similarity between spectral shapes for the proton, deuteron, and triton secondaries is demonstrated on Fig. 19 which shows the angle-integrated spectra for 60-MeV protons on ^{12}C, ^{54}Fe, and ^{120}Sn and 39-MeV protons on ^{54}Fe. This shape similarity has been previously noted at higher bombarding energies.[14,25,26] The ratio of intensities between the ^{1}H, ^{2}H, and ^{3}H spectra is A-dependent as discussed in the following section. However, while some of the data are less comprehensive than that presented here, the p/d ratio is ≈10/1 over a very wide energy range (40–350 MeV),[10,18,25] suggesting a common production mechanism which begs more thorough theoretical description.

In a recent publication Kalbach-Cline[35] has utilized the preequilibrium statistical model to calculate integral complex-particle spectra and

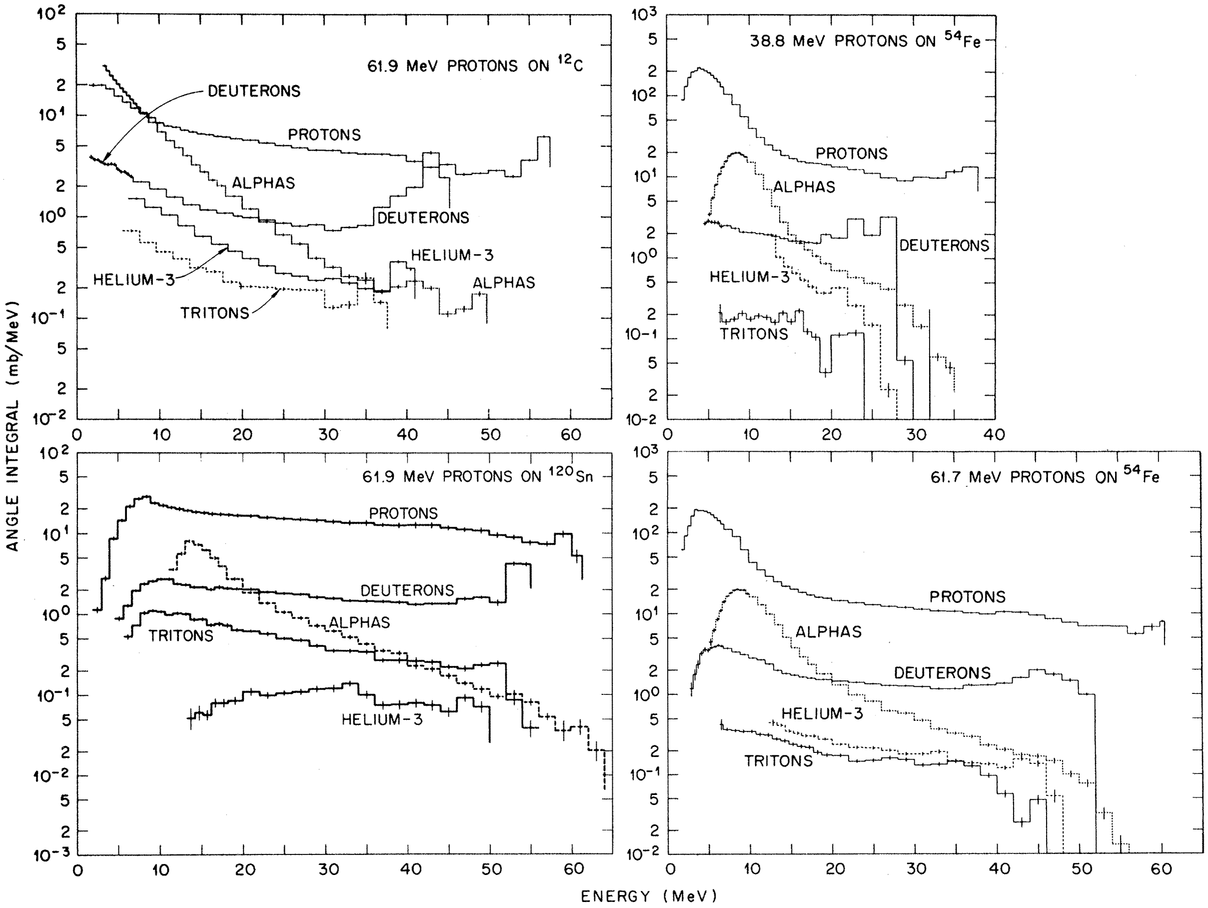

FIG. 19. Measured angle-integrated laboratory spectra of charged particles from ^{12}C, ^{54}Fe, and ^{120}Sn bombarded by 62-MeV protons and ^{54}Fe bombarded by 39-MeV protons. The spectra cover the entire measured energy range excluding elastic proton scattering. The spectrum of ^{3}He from ^{54}Fe at 39 MeV is uncertain by 25%.

has compared the predictions with our measured spectra. The calculation always provided significant high-energy cross sections and often produced excellent spectral shape agreement with the high-energy region of the integral spectra. These calculations tend to confirm that a preequilibrium mechanism is dominant in complex particle emission for energies studied here.

C. Mass Dependence

The nonevaporation continuum region can be taken as predominantly representing average nuclear properties rather than detailed nuclear structure if cross sections behave smoothly over a broad range of mass numbers and are independent of small mass number change. Figure 20 shows the ~40° (p, xp) spectrum from ^{54}Fe, ^{56}Fe, and ^{60}Ni bombarded by 62-MeV protons. While the high-energy peaks representing level structures and the low-energy evaporation cross sections are different for these three cases, the continuum shapes and magnitudes are the same within experimental uncertainty.

Figure 21 shows the mass dependence of the integrated cross section for each particle type studied. We have plotted cross sections for a given reaction type [i.e., (p, xd), etc.] over the same range of excitation energy for each target. In all cases the cutoff energy was set high enough to ensure that no evaporation contribution was made to the integral.

As can be determined from Fig. 21, the sum of $\sigma/A^{1/3}$ for all particle types for each target studied yields a rather constant value. Since the production of energetic particles is proportional to the nuclear circumference, these particles are interpreted as being produced predominantly in peripheral collisions.

The observed cross sections for protons are proportional within error to $A^{1/3}$ for $A \gtrsim 27$, while for the lighter targets there is a decrease in the number of high-energy protons from what would be expected from the data trend. The proton results of Roos and Wall[18] for the forward hemisphere at 160 MeV show the same mass dependence as shown by our data. The INC calculation predicts lower proton cross sections and a slightly different trend with mass for $A \gtrsim 27$, but predicts essentially correct integrated cross sections for

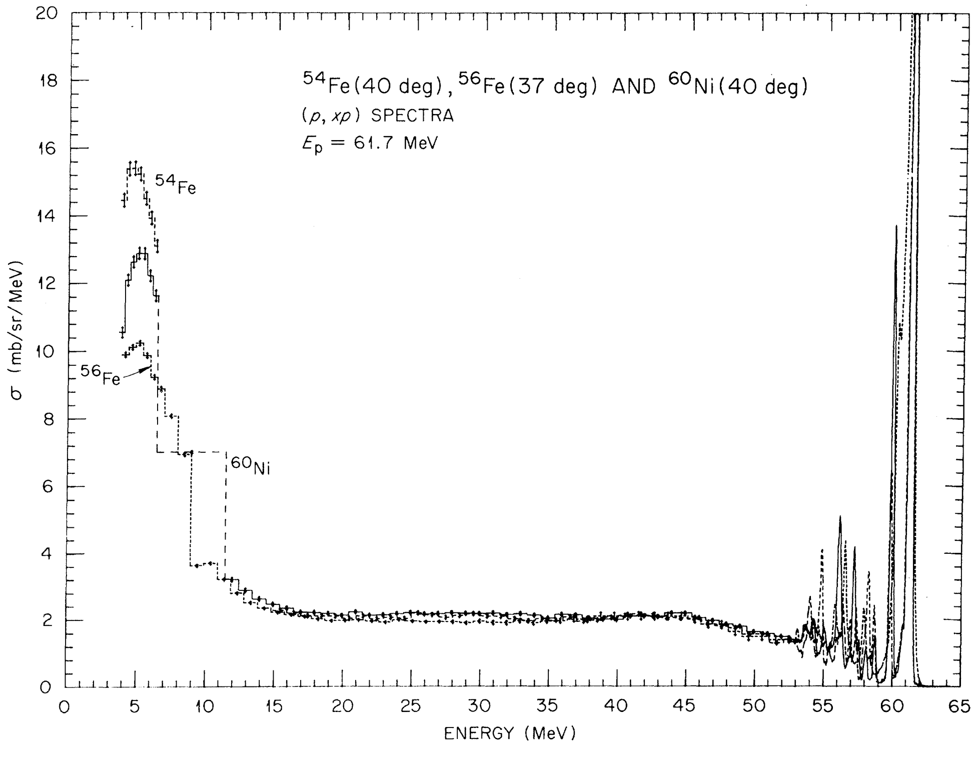

FIG. 20. Spectra from the (p,xp) reaction for 62-MeV protons on ^{56}Fe at 37° and on ^{54}Fe and ^{60}Ni at 40°. The broad dashed bin near 10 MeV in the otherwise solid line represents the average cross section for ^{60}Ni(p,xp) in the region where cross sections for this run were affected by a temporary "dead" layer in the detection system. A gap is shown in the ^{54}Fe(p,xp) curve from 6–15 MeV; beyond this energy the continuum cross sections are the same within uncertainty.

carbon and oxygen.

For $A \gtrsim 27$ the deuterons and tritons generally show an integral cross section proportional to $A^{1/3}$. The ratio $\sigma/A^{1/3}$ for α particles integrated over the indicated excitation energy region is found to be a strong function of target mass.

The ^{3}He cross section decreases strongly over the entire mass region studied. This decrease, which is independent of presentation method, is also evident in terms of the relative helium-3 to triton strength. For light targets we find more nonevaporation helium-3's than tritons, while for ^{209}Bi the helium-3 cross section is an order of magnitude less than that for the tritons. The decrease in the ^{3}He cross section as opposed to the constant triton cross section may represent the relative difficulty for removal of two protons from a very neutron-rich nucleus. Another interesting comparison of the ^{3}He and ^{3}H production is found in the ^{54}Fe and ^{56}Fe integrated cross sections shown on Fig. 21. The triton cross section from ^{54}Fe is nearly 50% larger than that from ^{56}Fe, while the inverse is the case for ^{3}He production.

Thus, while the proton and deuteron production from targets with $A \gtrsim 27$ varies smoothly as a function of mass, the production of triton, helium-3, and, at least for one case, α particles seems to be affected by nuclear structure.

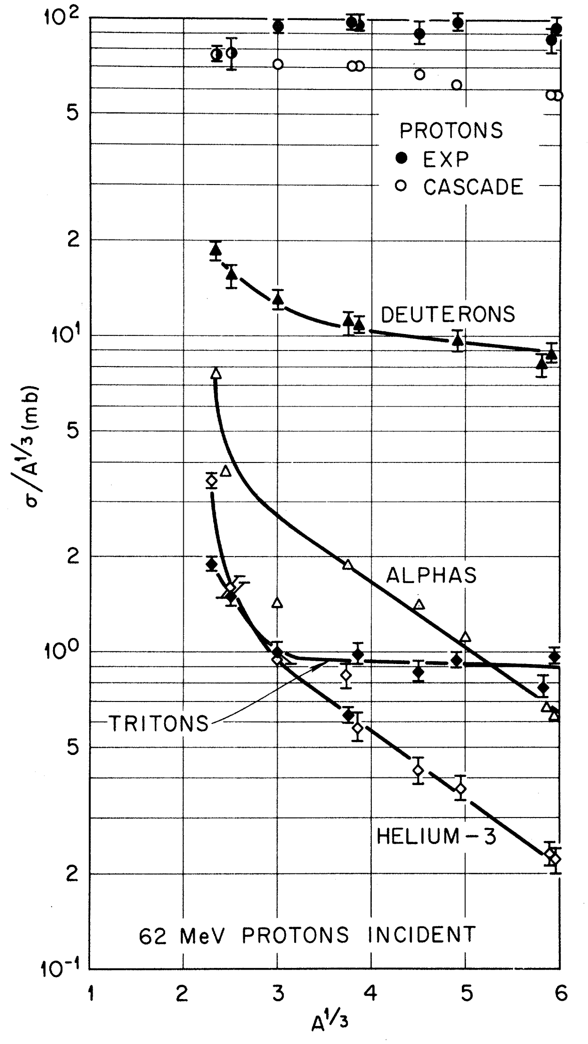

FIG. 21. Dependence of nonevaporation particle cross section on mass. The ordinate shows the measured cross sections divided by $A^{1/3}$ while the abscissa is plotted in units of $A^{1/3}$ for convenience. In order to compare cross sections for a given particle type over an equivalent energy range for each target, the measured cross sections were summed over the same excitation energy range for a given reaction on each target. The integral was obtained for the center-of-mass system and does not include elastic proton scattering. The excitation energy ranges used extend from 0 MeV to: p, 41 MeV; d, 25 MeV; t, 20 MeV; ^{3}He, 20 MeV; α particle 30 MeV. The cascade integrals shown are from the Bertini INC model.

D. Integral Results and Comparisons

Total Integrals

Listed on Table III are the measured yields of ^{1}H, ^{2}H, ^{3}H, ^{3}He, and ^{4}He particles for the three incident proton energies used. The yield is calculated as the measured particle cross section (integrated in this case over the entire nonelastic measured energy range) divided by the total reaction cross section for the incident channel (σ_R). To provide consistency for all the targets and energies used, we have chosen to use the σ_R values calculated by the Bertini INC model.[61] The integrated cross sections for protons from C, Al, Ni, and Bi measured with 57-MeV protons by Nonaka *et al.*[16] agree within ≈10% with our results. The results of Nonaka are given for exit energies above ≈15 MeV.

Since the results in Table III represent the entire energy spectra, in many cases the yields reflect the strong isotropic contribution from evaporation. For example, we have found that the angle-integrated nonevaporation spectra of the neighboring nuclei ^{54,56}Fe are identical in magnitude; however the integral yields are 2.0 and 1.3, respectively.

While the total charged-particle yield per inelastic event is nearly 2 for light and medium mass targets, the yields drop sharply for heavy targets as the Coulomb barrier rises. The same decrease in the importance of charged-particle emission from heavy nuclei is evident in Table IV where we show the energy per reaction carried off by ^{1}H, ^{2}H, ^{3}H, ^{3}He, and ^{4}He particles. While the charged particles from light targets account for 60–70% of the

TABLE III. Measured yields of charged particles above the cutoff energies shown. For all cases, except ^{3}H and ^{3}He, the cutoff energies are low enough to include essentially all particles emitted by the target. Elastic proton scattering is excluded. The σ_R values shown are those used to compute the yield and were obtained from the intranuclear cascade calculation (see Ref. 61). Unless otherwise noted, the uncertainty in the yield is 5–10% depending on the target.

Nucleus	Proton Y[a]	Proton COE[b]	Deuteron Y[a]	Deuteron COE[b]	Triton Y[a]	Triton COE[b]	Helium-3 Y[a]	Helium-3 COE[b]	α particle Y[a]	α particle COE[b]	σ_R (mb)
					62 MeV						
^{12}C	1.1	1.5	0.22	1.5	0.029	5.6	0.057	6.2	0.48	3.2	322
^{16}O	1.1	2.2	0.20	2.3	0.020	5.9	0.034	7.5	0.25	5.6	386
^{27}Al	1.3	2.4	0.17	2.4	0.017	6.2	0.021	6.7	0.31	2.9	537
^{54}Fe	2.0	1.7	0.11	2.4	0.008	6.3	0.012	7.3	0.18	4.9	822
^{56}Fe	1.3	3.8	0.10	4.8	0.015	5.9					846
^{89}Y	0.89	1.9	0.079	3.0	0.012	6.4	0.004	7.4	0.09	7.0	1125
^{120}Sn	0.60	2.0	0.070	4.6	0.017	5.6	0.002	13	0.047	11	1349
^{197}Au	0.36	3.6	0.048	4.8	0.012	6.4	0.001	13	0.018	13	1799
^{209}Bi	0.37	6.0	0.051	4.7	0.015	5.8	0.001	13	0.017	14	1876
					39 MeV						
^{12}C	0.79	2.8	0.17	3.0	0.009	5.7	0.048	13	0.39	5.5	382
^{54}Fe	1.68	1.6	0.059	3.0	0.003	6.3	0.008	12	0.13	4.4	918
^{209}Bi[c]	0.20	6.0	0.041	4.7	0.010	5.7	0.0004	13	0.008	14	2022
					29 MeV						
^{54}Fe	1.4	1.7	0.036	2.5	0.001	6.5	0.0004	13	0.099	4	973

[a] Y denotes yield which is particle production cross section (mb)/reaction cross section (mb).

[b] COE denotes cutoff energy (MeV).

[c] Uncertainty ≈20% for p, d, t, α; 50% for ^{3}He.

TABLE IV. Energy emitted per reaction in connection with charged-particle emission. The entire ^{1}H, ^{2}H, and ^{4}He spectra are included. For the light targets, the ^{3}H and ^{3}He yields are affected by ≈7-MeV cutoff energy. The reaction Q values have been included in the energy shown, but residual nucleus recoil energies have not been. Reaction probability was determined with the aid of σ_R values given by the Bertini INC calculation (see Ref. 61).

Nucleus	MeV/reaction
62 MeV	
^{12}C	42.5
^{16}O	34.9
^{27}Al	34.3
^{54}Fe	35.7
^{120}Sn	20.8
^{197}Au	14.2
^{209}Bi	14.8
40 MeV	
^{12}C	24.6
^{54}Fe	18.9
^{209}Bi	6.3
28 MeV	
^{54}Fe	13.3

available kinetic energy, the same particles emitted from ^{209}Bi account for only ≈25% of the energy.

A thin target (p, xn) experiment is currently under final analysis by Wachter *et al.*[57] Shown in Table V, along with our charged-particle data, are preliminary results for the kinetic energy per reaction carried off by the neutrons from the ^{27}Al(p, xn) reaction at 62 MeV. The low-energy cutoff for the neutron spectra is 9 MeV, thus excluding most of the evaporation contribution. It is seen that altogether ~52 MeV out of the available 62 MeV is accounted for, leaving 10 ± 4 MeV for low-energy neutrons and residual nucleus excitation and recoil. Also shown is an INC prediction for protons and neutrons. For both particle types the INC model underestimates the yield by ≈25%.

Table VI shows the importance of high-energy ($E > 20$ MeV) complex particle emission. The proton yields are normalized to 100 for ease of comparison; however, comparisons between targets should not be made except for cases of neighboring nuclei. For all cases studied at 60 MeV, the total complex-particle emission is at least 20% of that for protons, and for the lightest targets there are nearly 40% as many high-energy (nonevapora-

TABLE V. Energy balance for nonelastic reactions of 62-MeV protons on ^{27}Al. The results listed under total spectrum include all charged particles above the low-energy cutoffs in Table III, and the neutrons (see Ref. 57) were measured above a 9-MeV cutoff. The 20-MeV cutoff energy is sufficiently high to ensure that no evaporation contribution is made to the measurement or calculation. The reaction Q values have been included in the computations, but recoil and excitation of the residual nuclei have been excluded. Reaction cross sections were taken from the Bertini INC calculations (see Ref. 61).

Particle	Total spectrum Measured (MeV/reaction)	$E > 20$ MeV Measured Yield	$E > 20$ MeV Measured (MeV/reaction)	$E > 20$ MeV Calculated Yield	$E > 20$ MeV Calculated (MeV/reaction)
Protons	25.0	0.49	18.4	0.40	15.2
Deuterons	5.7	0.08	1.3	0	0
Tritons	0.6	0.007	0.10	0	0
Helium-3	0.7	0.008	0.16	0	0
α particles	2.3	0.02	0.61	0	0
Neutrons	17.9 ($E_n > 9$ MeV)	0.34	13.8	0.26	11.2
	52.2	0.95	34.4	0.66	26.4

tion) complex particles as protons. The high yield for the case of light targets may relate to the long discussed possible cluster character of these nuclei.

Proton Integral Results and INC Predictions

A comparison is made in Table VII between measured and INC calculated proton yields, average spectral energies, and energy yields per reaction. In addition, we show from Wachter[57] the same quantities for neutrons from ^{27}Al at 64 MeV. The calculated and measured average energies agree well. However, as shown by the percent difference in the last column, the Bertini INC model consistently predicts ≈30% too few high-energy protons (and neutrons for the one case analyzed) except for the lightest targets. Since the calculated yields are low, the calculated average energy per reaction carried off by high-energy protons is also low. This dearth of cascade energy release partially explains the excess computed proton evaporation cross section.

TABLE VI. Relative yields of ^{1}H, ^{2}H, ^{3}H, ^{3}He, and ^{4}He particles for $E > 20$ MeV. The proton yields are normalized to 100 to facilitate fractional production comparisons.

Nucleus	p	^{2}H	^{3}H	^{3}He	^{4}He	^{2}H + ^{3}H + ^{3}He + ^{4}He
			62 MeV			
^{12}C	100	23	2.1	3.8	7.7	36.6
^{16}O	100	22	1.6	2.7	6.3	32.6
^{27}Al [a]	100	16	1.4	1.6	4.1	23.1
^{54}Fe	100	12	0.8	1.2	3.8	17.8
^{56}Fe	100	13	1.5	(0.7)		
^{89}Y	100	13	1.6	0.8	4.2	19.6
^{120}Sn	100	13	2.3	0.6	3.8	19.7
^{197}Au	100	14	2.7	0.4	4.8	21.9
^{209}Bi	100	15	3.5	0.5	5.8	24.8
			40 MeV			
^{12}C	100	15	b	b	10.8	25.8
^{54}Fe	100	10	0.2	0.9	2.6	13.7
^{209}Bi	100	25	4.3	0.2	6.5	36

[a] The data of Wachter *et al*. (Ref. 57) imply a yield of 67 neutrons ($E > 20$ MeV) per 100 emitted protons.

[b] Due to the large negative Q values for these reactions, no particles of these types were observed with $E \geq 20$ MeV.

IV. CONCLUSIONS

Nonelastic reactions of 62-MeV protons produce charged secondary hydrogen and helium particles of over 20-MeV kinetic energy with a cross section of about $105A^{1/3}$ mb. The production is proportional to the nuclear circumference, so the particle yield per nonelastic reaction diminishes with increasing atomic weight. Only a small fraction of the reactions lead to excitation of bound states through reactions which emit a single particle. The variation of production cross sections and energy spectra of protons and deuterons of these energies is quite smooth with mass number. For targets heavier than aluminum, energetic deuterons and tritons have, respectively, about 10 and 1% of the secondary proton intensity and have similar spectra except for the "evaporation" region; for carbon and oxygen targets the complex-particle secondaries over 20 MeV amount to 40 and 34% of the corresponding inelastic proton intensity. The production of energetic helium particles falls with A and is not so smooth; thus, the relative behavior of tritium and ^{3}He particle production could be interesting for further study.

An equilibrium deexcitation or evaporation process seems important for secondary protons and perhaps α particles from some targets, but gen-

TABLE VII. Measured and calculated proton yields, average spectral energies, and energy per reaction for $E > 20$ MeV. The yields were calculated using the σ_R values shown in Table III. In the last column it is seen that for all but the lightest targets the intranuclear cascade calculation is deficient in high-energy proton and, at least for the ^{27}Al case, neutron prediction by 25–30%.

	Experiment [a]			Cascade calculation [a]			$(Y_{exp} - Y_{INC}/Y_{exp})$
	Yield	$\bar{E}$ [b]	MeV/reac [c]	Yield	$\bar{E}$ [b]	MeV/reac [c]	(%)
			62-MeV protons incident				
^{12}C	0.47	37.1	17.3	0.49	39.2	21.7	−4
^{16}O	0.44	35.8	16.0	0.47	39.1	18.1	−7
^{27}Al	0.49	37.8	18.4	0.40	38.1	15.2	18
^{27}Al(p,n) [d]	0.34	36.2	13.8	0.26	37.3	11.2	24
^{54}Fe	0.45	35.9	16.4	0.33	37.8	12.4	27
^{56}Fe	0.43	37.4	16.2	0.32	38.0	12.1	26
^{89}Y	0.35	36.8	12.9	0.27	38.1	9.7	23
^{120}Sn	0.37	38.5	14.1	0.23	38.3	8.7	35
^{197}Au	0.27	38.5	10.5	0.19	38.0	6.8	30
^{209}Bi	0.23	38.0	9.9	0.19	37.4	6.7	27
			39-MeV protons incident				
^{12}C	0.23	28.4	6.5	0.25	28.0	7.0	9
^{54}Fe	0.22	28.9	6.3	0.16	28.3	4.5	27
^{209}Bi	0.11	28.2	3.2	0.096	28.7	12.7	13

[a] $E > 20$ MeV. The Bertini INC model was used.

[b] $\bar{E} \equiv$ average proton energy.

[c] The reaction Q values have been included in the energy shown, but residual nucleus recoil energies have not been.

[d] Neutron yields as observed by Wachter *et al*. (Ref. 57).

erally the observed charged-particle spectra and angular distributions are quite unrelated to any prediction which could be derived from an equilibrium decay model. The differential cross sections for all particles are strongly anisotropic. While the average emerging energy diminishes greatly with increasing angle, intensity is observed to the highest kinematically allowed energy for a given nuclear reaction, even at a polar angle of 160° to the beam. A preequilibrium statistical model with a few free parameters can deal with the angle-integrated spectra and the relative intensities of the various secondaries, but no present model is known to describe quantitatively the angular distributions of the secondary complex particles in the continuum.

For secondary protons the intranuclear cascade model does provide detailed predictions of the observable differential cross sections and is known to yield the correct reaction cross sections in the energy region studied. Although the quasifree scattering peak predicted at small angles by some forms of the model is not observed, it is assumed that the underlying process is present but that the peak is smeared out over energy at a given angle by distorted wave and other effects in real nuclei.

Even though the de Broglie wavelength criterion usually given for the validity of the INC model is poorly met for the work described here, comparison with available experiments at higher energies is not complete enough to assure that agreement of the model with experimental data is more favorable than that demonstrated in this paper. The observed nonevaporation secondary proton intensity from the targets studied with 60-MeV incident protons is about 30% larger than that predicted by Bertini except for carbon and oxygen; however, the prediction is close to observation in the 25 to 50° range. We assume that the decrement of predicted cascade intensity, which necessarily leads to excess predicted intensity of evaporation protons, reflects an intrinsic difficulty of the cascade model, such as the assumption that hole excitations always lead to equilibrium decay. The cascade model always underestimates the intensity at very large and at very small angles. The former is taken to be the result of the model's neglect of short-range correlations or clustering among the bound nucleons. The latter, which shows a marked A dependence, deserves further study.

The results show that as the incident proton energy drops from 60 MeV, the observed differential cross sections smoothly merge toward the characteristics frequently observed at incident energies in the 20-MeV range. The chance of emission of two fast secondaries becomes small and there is relatively little secondary energy range in which to observe continuum behavior markedly different from that suggested by the evaporation model. Description of the reactions in conventional DWBA or coupled-channel language becomes increasingly appropriate as the incident energy is lowered.

The appearance of some broad structure in the unbound excitation region suggests possible success for a fresh description of reactions in this energy region by representing the first stage of the reaction process by a combination of collective interactions of various multipoles.

ACKNOWLEDGMENTS

Many have helped provide the results presented in this paper. We thank T. A. Love, N.W. Hill, R. Burrus, H. A. Todd, and C. O. McNew for help in system development; J. D. Drischler and E. Beckham for long hours of help with data analysis; and P. M. Aebersold and D. I. Putzulu for imaginative work on data analysis programs. M. P. Guthrie, B. L. Bishop, and J. L. Hardin helped run the many cases of the intranuclear cascade calculation. We thank M. B. Lewis for useful theoretical discussions. We wish to especially express our gratitude to H. W. Bertini for the invaluable theoretical assistance provided to us. We also thank G. D. Harp for providing the "VPOT" calculations and for helpful discussions. We thank R. G. Alsmiller, F. G. Perey, J. W. Wachter, H. W. Bertini, D. J. Horen, and G. D. Harp for careful review of the manuscript.

---

*Research sponsored by National Aeronautics and Space Administration Order L-12, 186 under Union Carbide Corporation's contract with the U.S. Atomic Energy Commission.

[1] F. E. Bertrand, J. K. Dickens, and T. A. Love, Phys. Lett. 24B, 653 (1967).

[2] F. E. Bertrand and M. B. Lewis, Nucl. Phys. A168, 259 (1971).

[3] M. B. Lewis and F. E. Bertrand, Nucl. Phys. A196, 337 (1972).

[4] D. M. Corley, N. S. Wall, H. Palevsky, J. L. Friedes, R. J. Sutter, G. W. Bennett, W. D. Simpson, G. C. Phillips, G. J. Igo, and R. L. Stearns, Nucl. Phys. A184, 437 (1972).

[5] L. S. Azhgirey, I. K. Vzorov, V. P. Zrelov, M. G. Mescheryakov, B. S. Neganov, R. M. Ryndin, and A. F. Shobudin, Nucl. Phys. 13, 258 (1958).

[6] J. W. Wachter, W. A. Gibson, and W. R. Burrus, Phys. Rev. C 6, 1496 (1972).

[7] J. B. Cladis, W. N. Hess, and B. J. Moyer, Phys. Rev. 87, 425 (1952).

[8] H. W. Bertini, Phys. Rev. 188, 1711 (1969).

[9] F. P. Kroll and N. W. Wall, Phys. Rev. C 1, 138 (1970).

[10] W. N. Hess and B. J. Moyer, Phys. Rev. 101, 337 (1956).

[11] R. D. Edge and H. H. Knox, Phys. Rev. 184, 1034 (1969).

[12] R. J. Sutter, J. L. Friedes, H. Palevsky, G. W. Bennett, G. J. Igo, W. D. Simpson, G. C. Phillips, D. M. Corley, N. S. Wall, and R. L. Stearns, Phys. Rev. Lett. 19, 1189 (1967).

[13] R. M. Eisberg and G. Igo, Phys. Rev. 93, 1039 (1954).

[14] J. Gênin, P. Radvanyi, I. Brissaud, and C. Detraz, J. Phys. Radium 22, 615 (1961).

[15] K. Strauch and F. Titus, Phys. Rev. 104, 191 (1956).

[16] I. Nonaka, T. Saji, A. Suzuki, H. Yamaguchi, R. Eisberg, Y. Ishizaki, K. Kikuchi, M. Matsuda, T. Mikumo, and Y. Nakajima, J. Phys. Soc. Jap. 17, 1817 (1962).

[17] C. Brun, H. Dubost, B. Gatty, M. Lefort, and X. Tarrogo, Nucl. Phys. A95, 337 (1967).

[18] N. S. Wall and P. G. Roos, Phys. Rev. 150, 811 (1966); P. G. Roos, Ph.D. thesis, University of Maryland, 1964 (unpublished).

[19] R. W. Peelle, T. A. Love, N. W. Hill, and R. T. Santoro, Phys. Rev. 167, 981 (1968).

[20] S. Dahlgren, D. Hasselgren, A. Imgemarsson, A. Johansson, P.-V. Renberg, and O. Sundgerg, Ark. Fys. 30, 510 (1965).

[21] H. Tyren and Th. A. J. Maris, Nucl. Phys. 4, 637 (1959); 6, 446 (1958); 7, 24 (1958).

[22] R. Fox and N. F. Ramsey, Phys. Rev. 125, 1609 (1962).

[23] L. E. Bailey, UCRL Report No. UCRL-3334, 1956 (unpublished).

[24] H. Dubost, M. Lefort, J. Peter, and X. Tarrago, Phys. Rev. 136, B1618 (1964).

[25] H. Dubost, B. Gatty, M. Lefort, J. Peter, and X. Tarrago, J. Phys. (Paris) 28, 257 (1967).

[26] M. Lefort, J. P. Cohen, H. Dubost, and X. Tarrago, Phys. Rev. 139, B1500 (1965).

[27] J. Muto, H. Itoh, K. Okano, N. Shiomi, K. Fukuda, Y. Omori, and M. Kihara, Nucl. Phys. 47, 19 (1963).

[28] J. J. Griffin, Phys. Rev. Lett. 17, 478 (1966).

[29] G. D. Harp and J. M. Miller, Phys. Rev. C 3, 1847 (1971).

[30] C. K. Cline and M. Blann, Nucl. Phys. A172, 225 (1971).

[31] M. L. Goldberger, Phys. Rev. 74, 1269 (1948).

[32] N. Metropolis, R. Bivins, M. Storm, A. Turkevich, J. M. Miller, and G. Friedlander, Phys. Rev. 110, 185 (1958).

[33] M. Blann, Phys. Rev. Lett. 28, 751 (1972).

[34] M. Blann and A. Mignerey, Nucl. Phys. A186, 245 (1972).

[35] C. K. Cline, Nucl. Phys. A193, 417 (1972).

[36] H. W. Bertini, Phys. Rev. 131, 1801 (1963); 138, B2 (1965); 188, 1711 (1969).

[37] V. S. Barashenkov, K. K. Gudima, and V. D. Toneev, JINR Report No. P2-4066, 1968 (unpublished); JINR Report No. P2-4065, 1968 (unpublished); Acta Phys. Pol. 36, 415 (1969).

[38] K. Chen, G. Friedlander, G. D. Harp, and J. M. Miller, Phys. Rev. C 4, 2234 (1971); Phys. Rev. 176, 1208 (1968); 166, 949 (1968).

[39] V. S. Barashenkov, H. W. Bertini, K. Chen, G. Friedlander, G. D. Harp, A. S. Iljenov, J. M. Miller, and V. D. Toneev, Nucl. Phys. A187, 531 (1972).

[40] L. Dresner, ORNL Report No. ORNL-CF-61-12-30, 1961 (unpublished).

[41] V. F. Weisskopf, Phys. Rev. 52, 295 (1937).

[42] I. Dostrovsky, Z. Frankel, and G. Friedlander, Phys. Rev. 116, 683 (1959); 118, 781 (1960); 118, 791 (1960).

[43] H. W. Bertini, Phys. Rev. C 6, 631 (1972); 1, 423 (1970); Phys. Lett. 30B, 300 (1969); Phys. Rev. 131, 1801 (1963); 138, B2(E) (1965).

[44] F. E. Bertrand, to be published.

[45] B. H. Bransden, Proc. Phys. Soc. Lond. A65, 738 (1952).

[46] S. T. Butler and C. H. Pearson, Phys. Rev. 129, 836 (1961).

[47] F. E. Bertrand, W. R. Burrus, N. W. Hill, T. A. Love, and R. W. Peelle, Nucl. Instrum. Methods 101, 475 (1972); F. E. Bertrand, R. W. Peelle, T. A. Love, N. W. Hill, and W. R. Burrus, ORNL Report No. ORNL-4274, 1968 (unpublished).

[48] N. W. Hill and W. P. Albritton, Nucl. Instrum. Methods 75, 18 (1969).

[49] F. E. Bertrand and R. W. Peelle, ORNL Report No. ORNL-4799 (to be published).

[50] F. E. Bertrand, R. W. Peelle, T. A. Love, R. J. Fox, N. W. Hill, and H. A. Todd, IEEE Trans. Nucl. Sci. NS-13, 279 (1966).

[51] For $A=3$ particles the mass ambiguity in time-of-flight (TOF) limits the t and ^{3}He low-energy cutoff to ≈6 MeV. For other particles, a combination of target thickness and heavy particle recoil foldover ambiguity in the TOF system limited the low-energy cutoffs to between 1.5–5 MeV. For all but the lightest targets, these cutoffs provide coverage of the entire spectrum.

[52] F. E. Bertrand and R. W. Peelle, ORNL Report No. ORNL-4450, 1969 (unpublished); ORNL Report No. ORNL-4471, 1970 (unpublished); ORNL Report No. ORNL-4455, 1969 (unpublished); ORNL Report No. ORNL-4460, 1969 (unpublished); ORNL Report No. ORNL-4469, 1970 (unpublished); ORNL Report No. ORNL-4638, 1971 (unpublished); ORNL Report No. ORNL-4698, 1971 (unpublished); ORNL Report No. ORNL-4456, 1969 (unpublished).

[53] S. Fukuda and Y. Torizuka, Phys. Rev. Lett. 29, 1109 (1972).

[54] G. R. Satchler, Nucl. Phys. A195, 1 (1972).

[55] G. R. Satchler, Particles and Nuclei (to be published).

[56] The authors wish to thank G. D. Harp for providing the calculated spectra from the Brookhaven intranuclear cascade code VEGAS.

[57] The neutron results were kindly supplied to us prior to publication by J. W. Wachter. Preliminary results and some experimental details for the (p,xn) experiment may be found in J. W. Wachter, R. T. Santoro, T. A. Love, and W. Zobel, Bull. Am. Phys. Soc. 18, 118 (1973).

[58] The authors wish to thank H. W. Bertini for temporarily modifying the cascade program.

[59] J. J. H. Menet, E. E. Gross, J. J. Malinify, and A. Zucker, Phys. Rev. C 4, 1114 (1971).

[60] E. Gadioli, I. Iori, N. Molko, and L. Zetta, Nuovo Cimento Lett. 3, 677 (1972).

[61] H. W. Bertini, Phys. Rev. C 5, 2118 (1972).